NEW CONSTRAINTS ON TIMING AND MECHANISMS OF REGIONAL TECTONISM FROM MERCURY'S TILTED CRATERS. Jeffrey A. Balcerski[1], Steven A. Hauck, II[1], Peng Sun[1], Christian Klimczak[2], Paul K. Byrne[2], Roger J. Phillips[3], and Sean C. Solomon[2,4]; [1]Dept. of Earth, Environmental, and Planetary Sciences, Case Western Reserve University, Cleveland, OH 44106 (jeffrey.balcerski@case.edu); [2]Dept. of Terrestrial Magnetism, Carnegie Institution of Washington, Washington, DC 20015; [3]Planetary Science Directorate, Southwest Research Institute, Boulder, CO 80302; [4]Lamont-Doherty Earth Observatory, Columbia University, Palisades, NY, 10964.

Introduction: Analysis of altimetry and images from MESSENGER indicate that Mercury's surface exhibits both a relatively low dynamic range of topography and broad regions of low-amplitude, long-wavelength, undulatory terrain [1, 2]. The cause of these undulations is unclear, though lithospheric folding [3], volcanic intrusion, and isostatic compensation processes have been invoked. Impact craters are one of the most evident and ubiquitous features of terrestrial bodies, and often serve as useful indicators of regional tectonic deformation [4−6]. Since impact melt within suitably large craters is expected to follow an equipotential surface until solidification, those for which the floor is inclined from the horizontal have likely undergone deformation after formation [e.g., 2]. With the abundant flat-floored craters on Mercury, we explore the relationship between these craters and the long-wavelength topography, with the goal of better characterizing its development.

Approach: Using orbital images from the Mercury Dual Imaging System (MDIS), we identified craters with a fresh appearance and whose floors appear flat. That is, we cataloged craters with sharp rims, a visible contact between the interior wall and the crater floor, and the absence of ejecta and interior tectonic features such as faults or ridges [e.g., 7, 8]. We included craters that may have been volcanically flooded but which have discernible flat interior floors, and distinguish between these and fresher craters (with interior floors suggestive of impact melt origin) during a morphologic analysis. As a final step in the image analysis, we assigned a morphological classification (C_1-C_5) to the craters, following McCauley et al. [9], where C_5 is the best preserved. This process was facilitated by the use of a combination of high-albedo and high-relief MDIS base map mosaics, which allowed for visualization of both fine topographic features and reflectance differences that help identify ejecta, impact melt, and recent surface excavation. Our database includes craters that have either single or multiple Mercury Laser Altimeter (MLA) tracks across their floors, providing a large dataset of along-track floor tilt measurements and a smaller set of true slope measurements. Taking MLA shot returns only from the high-threshold, high-integration window, we manually selected those that were judged from images to represent the crater floor. We determined a best-fit plane to these points, which allowed comparison and benchmarking of "true" slope, with those resulting from the along-track projections. In order to compare the measured crater tilts with regional slopes, we obtained the direction and magnitude of maximum topographic gradient at a baseline of 1° (~40 km) from the center of each measured MLA segment. These topographic gradients were obtained using topography models of spherical harmonic degree and order through 20, 50, and 80, which effectively removed high-frequency, small-scale topography and enabled us to explore the relationship between modified craters and Mercury's long-wavelength features.

The use of craters as indicators of topographic evolution involves distinguishing the effects of crater morphology, age, altimetric track length, quality of coverage, and underlying local and regional effects, such as faulting, folding, and volcanism. The reference to which slopes are measured may be equally important, since the definition of "level" depends on the gravitational equipotential, which can differ from simple spheroidal or ellipsoidal models of terrestrial bodies.

Results: The complete dataset (1,300 measurements) of crater floor slopes with at least one MLA track is shown in Fig. 1. These data exhibit a strong, unimodal concentration near horizontal, with a standard deviation of 0.3°, and show no evidence of a northward or southward bias. The long-wavelength topographic features have similar slope magnitudes. For instance, the maximum gradient for spherical harmonic model of l=50 (~300 km) in the northern hemisphere is 1.1°. These magnitudes are also similar to craters in the Beta-Atla-Themis region of Venus [6]. We further find that the maximum magnitude of difference between sphere-referenced and geoid-referenced slopes is only 0.02°. Thus, the current geoid of Mercury is insufficient to explain any measurable portion of the observed crater tilts.

We can also address the question of whether the differential height of a crater's rim might also be useful for similar studies. MLA profiles along craters superposed on others, such as the example shown in Figure 2, provide evidence that the profile of a crater rim and ejecta blanket can be the result of underlying, pre-existing topography, making these features less useful for these studies than the interior crater floors.

Finally, a comparison of measured crater slopes and long-wavelength topographic slopes in the northern hemisphere is not uniquely suggestive of a dominant deformation event during Mercury's evolution. Rather, the processes that led to long-wavelength topographic changes, such as the northern rise and those within the Caloris basin, are the result of multiple regional events and/or processes that operated continuously throughout much of the planet's history.

Caloris: The event that formed the Caloris basin presumably erased pre-existing topography, and so the presence of expansive, undulating terrain cross-cutting the northern and southern portions of the volcanically filled floor [1, 2] is unexpected. Existing superposed craters within the basin postdate interior plains emplacement. Studies of the abundant tectonic features within the basin reveal no clear correlation between faulting and the long-wavelength topography [10, 11], so crater floor tilt measurements may be particularly valuable in understanding the topographic changes within Caloris. From the along-track and plane-fit measurements we find that even some C_4 and C_5 craters have been tilted in directions and magnitudes that closely follow that of the long-wavelength topography (Figure 3). We therefore hypothesize that this topography developed comparatively recently in Mercury's geologic history.

Northern Plains: An isolated, broad topographic rise in the northern volcanic plains [2, 12−14] contains both fresh and buried impact craters. We find that the fresh craters have markedly shallower slopes than both the spherical harmonic models and buried craters, and those with floors departing from horizontal follow the same outward-dipping trends as older craters. We interpret these observations as arguments that this topographic feature postdated northern plains emplacement but ceased further modification before the time of formation of the younger superposed craters. The rise was unlikely to have been formed by volcanic construction, because buried craters appear to maintain a constant depth (relative to rim height) on both their upslope and downslope sides.

References: [1] Oberst, J., et al. (2010) *Icarus 209,* 230. [2] Zuber, M. T., et al. (2012) *Science 336,* 217. [3] Dombard, A. J., et al. (2001) *LPS 32,* #2035. [4] Roth, L. E., et al. (1981) *LPS 12,* #906. [5] Stoddard, P. R., et al. (2003) *LPS 34,* #2129. [6] Matias, A., et al. (2005) *GSA Special Paper 388.* [7] Kalynn, J. D., et al. *GRL in press.* [8] Ostrach, L. R., et al. (2012) *LPS 43* #1113. [9] McCauley, J. F., et al. (1981) *Icarus 47,* 181. [10] Klimczak, C, et al. (2012) *EPSC 7, #751.* [11] Byrne, P. K., et al. (2012) *LPS 43* #1722. [12] Solomon, S. C., et al. (2012) *LPS 43* #1578, [13] Dickson, J. L., et al. (2012) *LPS 43* #2249. [14] Klimczak C. et al. (2012) *JGR, 117,* E00L03.

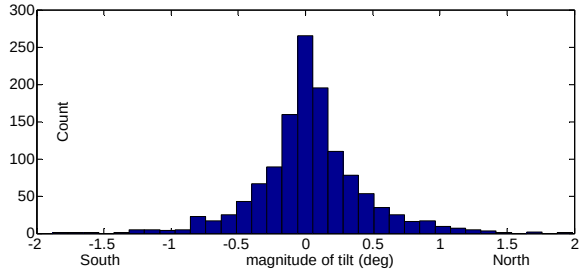

Figure 1. Histogram of all along-track crater floor tilt measurements.

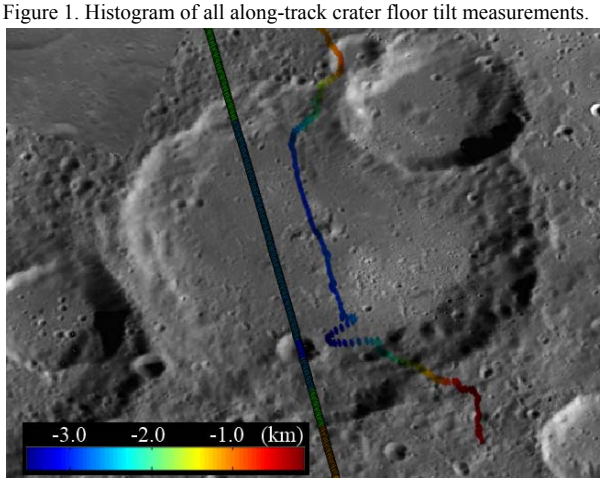

Figure 2. MLA profile and relative topography projected perpendicular to the ground track through an unnamed 80 km diameter crater (39.4°N, 31.9°E) and superposed crater on its interior wall.

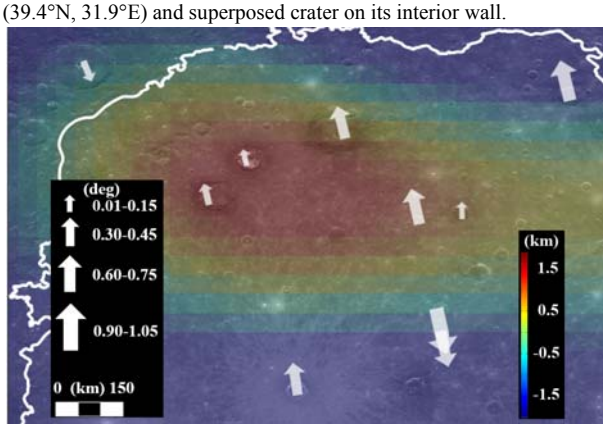

Figure 3. Plane-fits of craters in northern Caloris, showing fresh craters tilted away from topographic high (color shaded for spherical harmonic through n=20; basin outline in white).